Res. Rep. Fac. Eng. Mie Univ., Vol. 14, pp. 57-82 (1989)

Original Paper

Experimental Study on Elasto-Plastic Behavior of Steel Reinforced Concrete Space Frames

Shosuke MORINO, Jun KAWAGUCHI
and Chihiro YASUZAKI
(Department of Architecture)

(Received September 16, 1989)

Elasto-plastic behavior of steel reinforced concrete (SRC) space frames subjected to constant axial thrust and repeated biaxial bending with shear is investigated experimentally, in order to establish an evaluation method for the earthquake resistance ability of SRC structures. Frame specimen consists of a column and four beams arranged in two directions, which modelizes beam-and-column subassemblage in a real building frame. Cross sections of members are made of H-steel (column:2H-150x30x6x9, beam:H-180x50x6x9) and four main reinforcements encased in concrete. In the test, constant vertical load at the column top and constant beam loads at tips of beams in one-direction are first applied, the latter simulating the long-term load. Then, anti-symmetric, alternately repeated shear loads are applied at tips of beams in the other-direction simulating the earthquake load. Experimental parameters selected are axial thrust ratio, intensity and pattern of beam loads corresponding to the long-term load, and failure modes (column-failure type and panel-failure type). The paper discusses the effect of three-dimensional loading on the maximum strength, deformation capacity, energy dissipation capacity, and failure modes, with presenting the test results.

Key Words: Steel reinforced concrete frame, three-dimensional loading, maximum strength, deformation capacity, energy dissipation

1. INTRODUCTION

Steel reinforced concrete (SRC) column in Japan is rather stocky, since working stresses under the earthquake loading are large and control the design. Therefore, most of the researches on SRC columns carried recently in Japan have put emphasis on the shear behavior of short columns, particularly after reinforced concrete short columns were badly damaged by Tokachi-oki Earthquake in 1968. Researches on slender SRC columns have been carried out mainly in

Europe, which were reviewed by Stevens [1] and Bridge and Roderick [2], and very few had been done in Japan. As to the biaxial bending problems of SRC columns, Morino and Matsui [3,4] presented literature surveys.

Beam-and-column subassemblage in a multi-story frame under the earthquake is subjected to repeated flexure with shear about one-axis due to earthquake horizontal loading, in addition to constant axial thrust and flexure about the other axis. Therefore, the column as well as the beam-to-column connection are in the three-dimensional stress state. Researches on the beam-to-column connection of SRC structure are thoroughly reviewed by Wakabayashi and Minami [5,6], which reveals that no research has been found on the three-dimansional behavior of SRC connections. The purpose of this research is to investigate the overall elasto-plastic behavior of three-dimensional beam-and-column subassemblage, subjected to axial thrust and bi-directional beam loads, and clarify the effect of three-dimensional loading on the maximum strength, deformation capacity and energy dissipation capacity.

2. EXPERIMENTAL INVESTIGATION

2.1 Specimen

Figure 1 is schematical illustration of a specimen and loading condition. A constant axial thrust P is applied on the centroid of the column top section, and constant vertical loads W1 and W2, which simulate long-term loading, are applied at the tips of short beams (beam B). A couple of anti-symmetrical vertical load Q are repeatedly applied at the tips of long beams (beam A), simulating the earthquake load. Experimental parameters vary as follows: failure types (column-failure type or panel-failure type); pattern of beam loads corresponding to the long-term load (balanced or unbalanced load); and intensity of the axial thrust P (40ton or 80ton). Table 1 shows the correspondence between the value of each parameter and the name of specimen.

Figure 2 shows the shape and size of specimen. Cross sections of beams and column are shown in Fig. 3. The steel portion of beam A is passing through, and beam B and column are welded to beam A. Beams have H-shaped section (H-180x50x6x9) built-up from flange (9 mm) and web (6 mm) plates by welding. Column is formed to cross-H section (2H-150x100x6x9) by welding from two rolled H-shaped steel (H-150x100x6x9) of which flange tips are cut off by flame-cutting. Specimens are not annealed. Column steel is encased in the square concrete 230x230 mm with 4 deformed steel bars (D10) and hoops (D6) placed with a pitch of 100 mm. Beams are encased in the rectangular concrete 230x300 mm with 4 deformed bars (D16) and stirrups (D6) placed with a pitch of 120 mm. Panel of the beam-to-column connection of C-series specimens (column-failure type) are strengthened by hoops and doubler plates of 2-PL9. Figure 4 shows the beam-to-column connections. Table 2 shows the average values of mechanical properties obtained from the coupon test of steel and the cylinder test of concrete. Coupons of flange and web of column are taken from rolled-H section after flame-cutting of flange tips, which is under the same heat-treatment condition as the specimens.

2.2 Test Set-up

Figure 5 shows the test set-up. The specimen ① is set in the loading frame ② and top and bottom of the column are supported by ball-bearings ③. All beams are connected to mechanical screw jacks ④ with H-shaped steel members ⑤. The specimen is supported at the top by 4 horizontal braces ⑥. First, the constant axial thrust P is loaded on the top of the specimen by a hydraulic jack ⑦. The constant vertical loads on beam B (W1 and W2) are applied next, and then the alternately repeated vertical loads on beam A (Q) are applied controlling the displacement amplitude to be prescribed value.

Figure 6 shows the position of the displacement meters. D1 and D2 measure the relative displacements of column against beam A, which are placed on the measuring frame supported at the points 8 cm inside the load points of beam A. D3 and D4 measure the absolute displacements of beam A at the supporting point of the measuring frame. The deofrmed configuration of the specimen and the measuring system are schematically shown in Fig. 7. All loads, i.e., constant axial trust, constant vertical loads and repeated vertical loads, are measured by load cells ⑧ attached to each jack. Wire strain gauges are mounted on the steel portion and reinforcing bars of the column.

The procedure of alternately repeated loading on beam A is as follows: The specimen is first subjected to two cycles of alternately repeated beam A load, with controlling the amplitude of average displacement of D1 and D2 to be equal to ±10 mm, and the controlling displacement amplitude is increased by the amount of ±10 mm, after every two cycles of loading are completed.

2.3 Test Results

2.3.1 Load-Displacement Behavior

Figure 8 shows the relations between the load Q on beam A and the average value of column displacements D1 and D2 of all specimens. Specimens in C-series fail with the flexural failure of the column, while those in P-series shows the failure of beam-to-column connection panel. Specimens with 31 and 11 as the last two digits of numbers in their names are subjected to three-dimensional loading. Columns of the specimens with 11 and 00 are under uniaxial bending condition, and those with 31 are subjected to biaxial bending. Intensities of the axial thrust P equal to 40 and 80 ton approximately correspond to the axial thrust ratio 0.2 and 0.4 in C-series, and 0.15 and 0.3 in P-series, respectively.

C-series: Hysteresis loops of all specimens show the pinched-shape as observed in the reinforced concrete structures, at first few cycles of loading. Then, they gradually shift to the spindle shape as in the steel structures. Hysteresis loops of C4000 shows quite stable spindle shape, while those of C4011, C4031 and C8031 become rather slender and thus the energy dissipation capacity becomes smaller compared with C4000. Every specimen reaches the state of maximum strength in the first loading cycle with the amplitude ±20 mm, or in between ±20 and ±30 mm. Before reaching the maximum strength, the strength deterioration in the second cycle of loading in the same amplitude is not very

large, but it becomes drastically large in the loading cycles after the maximum strength. Each test was terminated, when the specimen became unable to sustain the constant axial thrust. The time of termination becomes earlier in the order of C8031, C4031, C4011 and C4000. C8031 and C4000 show the smallest and the largest deformation capacity, respectively. Maximum strength appears at the negative loading side except C4031. The strength deterioration observed in the course of increasing the displacement amplitude after the maximum strength is rather large in the specimens subjected to three-dimensional loading, compared with C4000. Not only biaxial loading but also three-dimensional loading cause more drastic deterioration of strength and deformation capacity.

P-series: Concrete strength of P-series specimens is much higher than those of C-series, and thus the maximum strength becomes higher. As observed in C-series, histeresis loops show the pinched-shape at first, then shift to the stable spindle shapes. Tendency in the deterioration of strength and deformation capacity is nearly the same as observed in C-series. However, compared with C-series, hysteresis loops of P-series specimens become more stable spindle shape, indicating better energy dissipation capacity. Again, P4000 shows the largest deformation capacity and P8031 the smallest, but P4000 could sustain the axial thrust until the end of test, which was terminated because of the short stroke of loading jacks. Three-dimensional loading decreases the deformation capacity, but it seems to give no effect on the strength, comparing P4000 with P4011. Biaxial bending affects on the strength deterioration, comparing P4031 with P4011.

Figure 10 shows the load-strain relations of which strain data are obtained from the wire strain gauges mounted on the steel portion shown in Fig. 9. Gauge 1 is for the flange strain of the lower column subjected to compression by bending at virgin loading. Gauges 2 and 3 are horizontal strains of panels of A and B-directions, respectively. In all specimens, the flange of the lower column yields, and the Q-ε loops for the flange strain drift away to one direction apart from the origin, except for C4000. The loops of C4000 show the anti-symmetric spindle shape, while the strain accumulation causes the deterioration of strength and deformation capacity in all other specimens. Gauge 1 of C4031 does not show large strain, but the opposite flange is subjected to severe yielding in this case, although the data are not shown in the figure. The panels of C-series specimens all behaves elastically until the end of the test. Especially the strains in B-direction panels are nearly zero. Among the specimens in P-series, the panels of P4031 and P8031 yields and the Q-ε loops show anti-symmetric spindle shape, while the panel strain of P4011 and P4000 does not become too large, just exceeding the yield strain. Drifting phenomenon observed in the flange strain is not observed in Q-ε loops for the panel strain.

2.3.2 Failure Modes

a) Crack patterns

Figure 11 shows the sketch of crack patterns of specimens C4000, C4031, P4031 and P8031 at the end of experiment, since crack patterns of C4011, C4031 and C8031 are similar, and those of P4011, P4000 and P4031 are also similar. Shaded area in the sketch of cracks indicates the area in which the concrete

failing in compression spalls off. C4000 shows the concrete damage in sandglass shape on lower column only, while the upper and lower columns of C4031 are equally damaged by flexure. In the case of C4031, the damaged portion does not become the sandglass shape, because of the biaxial bending. Specimens P4031 and P8031 show the damage in the upper and lower columns, among which the damages on the lower column are fatal in the case of P4031. Cracks are not observed in beams, but rather wide cracks to separate the beam end from the column surface are observed in P4031 and P8031, which are not observed in C-series.

b) Failure modes

Figure 12 shows the relations between the displacement at the top and the base of the column, D1 and D2. Note that the shapes of D1-D2 curves are separated into two patterns: The one shows anti-symmetrical spindle shape as observed in P-series specimens except for P8031, in which only D2 exhibits the large value while D1 stays within rather small value. The other pattern shows D1-D2 curve drifts away from the origin after few cycles of loading, which is observed mainly in C-series specimens except for C4000. In Fig. 13, the relations between the load Q and the displacement D1 or D2 are drawn to explain two patterns in D1-D2 curves more clearly. In the case of the first pattern, which shows anti-symmetrical spindle shape of D1-D2 curve in Fig. 12, the Q-D1 relation shows rather linear behavior with small amplitude of D1, while the Q-D2 relation shows spindle shaped loop with large amplitude of D2, as observed in C4000 and P4031 in Fig. 13. Deformed configurations at the turning points of positive and negative loading sides are schematically illustrated in Fig. 14 (a) for a specimen exhibiting anti-symmetrical type of displacement behavior, in which a plastic hinge forms at the top of the lower column only, and the lower column displacement D1 relative to the beam tips is mainly caused by the rotation of the plastic hinge, all other portion moving as a rigid body. The specimen of this type shows symmetrical doglegged configuration at the turning points in one cycle of loading, and the center of the beam-to-column connection symmetrically moves back and forth on the horizontal line. In the case of the second pattern of drifting type shown in Fig. 12, Q-D1 and Q-D2 relations become as shown in Fig. 13 for C4031 and P8031. Note that Q-D1 and Q-D2 curves are quite similar if either one of these two curves is placed up-side down. Deformed configurations of a specimen of this type at the turning points in one cycle of loading are as shown in Fig. 14 (b), in which plastic hinges from at both ends of the upper and the lower columns. In the positive loading, the hinge at the end of the lower column mainly rotates and the value of D2 becomes large while D1 stays within the small value, and the hinge in the upper column mainly rotates in the negative loading causing large value of D1. Doglegged configuration is fixed in one-way, and the center of the beam-to-column connection gradually drifts away to one-direction.

3. DISCUSSIONS

3.1 Ultimate Strength

Ultimate strength of each specimen is shown in Fig. 8, where solid line

indicates the ultimate flexural strength of column and dotted line the ultimate shear strength of beam-to-column connection.

a) Ultimate flexural strength of column

The ultimate flexural strength of C-series specimens is calculated by the superposed strength method based on measured dimensions and mechanical properties of materials shown in Tables 2 and 3. The actual calculation of the column strength subjected to uniaxial bending is done by the formulas and computer programs presented in Refs. [7] and [8].

The ultimate flexural strength of column subjected to axial force and biaxial bending is calculated by Eq. (1) suggested in Ref. [8], substituting the strength for uniaxial bending obtained by the programs in Ref. [7].

$$\bar{M}_x^{\alpha} + \bar{M}_y^{\alpha} = 1.0$$

$$\bar{M}_x = M_x / M_{xo},\ \bar{M}_y = M_y / M_{yo} \qquad (1)$$

$$\alpha = 3.30\bar{n}^2 - 1.42\bar{n} + 1.74 \quad : \text{for single H-shaped steel section}$$

$$\alpha = 2.0 \quad : \text{for cross-H-shaped steel section}$$

$$\bar{n} = N / N_{max}$$

where,

M_{xo}, M_{yo}: superposed strength of column subjected to axial force and uniaxial bending

M_x, M_y : bending moments about x-and y-axis, respectively

N : axial force

N_{max} : ultimate axial strength

The column moment calculated by Eq. (1) is converted to the load on the tips of beam A, and shown by solid lines in Fig. 8.

b) Ultimate shear strength of beam-to-column connection

Panel moment determined by ultimate shear strength of the beam-to-column connection for P-series specimens is calculated by Eq. (2) specified in SRC Standard [9].

$$_JM_u = {}_cV_e({}_JF_s \cdot {}_J\delta + {}_wp \cdot {}_w\sigma_y) + 1.2\,{}_sV \cdot {}_s\sigma_y / \sqrt{3} \qquad (2)$$

where,

$_JF_s$: shear strength of concrete

$_cV_e$: effective volume of beam-to-column connection

$_J\delta$: shape factor of connection panel, taken equal to 3 in this case

$_wp$: hoop ratio

$_w\sigma_y$: yield stress of hoops

$_sV$: volume of steel panel plate

$_s\sigma_y$: yield stress of steel panel plate

The panel moment calculated by Eq.(2) is converted to the load on the tips of beam A, and shown by dotted lines in Fig. 8. Effects of biaxial bending are not considered.

3.2 Discussions

a) Ultimate strength

Ultimate strength of C-series specimens is calculated as the ultimate flexural strength of column subjected to axial force and bending. It is observed from Fig. 8 that the maximum strength of any specimen in C-series attained in the positve loading cycle does not reach the calculated ultimate strength, although the maximum strength in the negative loading cycle exceeds the calculated value in some cases. Several reasons of this matter are considered: unbalanced loads on beam A caused by the slip of bolts connecting beam A and steel member around the peak load; use of average values of cross-sectional dimensions for the calculation; difference in concrete strengths of the specimen and the cylinder, caused by concrete-casting with the standing position of columns; error involved in simplified formula for biaxial bending strength, Eq. (1); and P-Δ effect due to the movement of the connection, which is neglected in the calculation. Comparing the maximum strength of each specimen in C-series, the strengths of C4000 and C4011 are nearly equal, and that of C4031 is larger than the former two.

Ultimate strengths corresponding to column failure and panel failure are both shown in Fig. 8 for P-series specimens. The maximum strength of every specimen does not reach the ultimate strength determined by column failure. The maximum strength of two specimens subjected to uniaxial bending in P-series is well estimated by the ultimate shear strength of the beam-to-column connection panel given by Eq.(2), while the strength those subjected to biaxial bending does not reach the predicted strength. Note that the maximum strength of P4031 is smaller than nearly identical strength of P4000 and P4011. Therefore, it is confirmed that the strength of the connection panel is decreased by the effect of biaxial bending.

b) Load-displacement behavior

Among the specimens in C-series, the energy dissipation capacity of C4000 is obviously much larger than others, and C8031 shows rather brittle failure. The envelop curves for the load-displacement loops in the positive loading side indicate that the negative slope of the curve after the maximum strength becomes steeper in the order of C8031, C4031, C4011 and C4000, which agrees with the order of the amount of displacement amplitude achieved at the termination of the test. Therefore, it seems that three-dimensional loading and biaxial bending give bad effects on the deformation capacity and energy dissipation capacity.

Behavior of brittle failure shown by C8031 may be caused by the greater P-Δ effect due to the horizontal movement of the beam-to-column connection. Observing the envelop curves for the loops in the positive loading, the deformation capacity and energy dissipation capacity of P-series specimens are better than C-series specimens, and it may be said that the panel-failing type is more advantageous than the column-failing type. The maximum strengths and the deformation capacities of the specimens subjected to uniaxial bending, i.e, P4000 and P4011, are almost on the same level, and the effect of three-dimensional loading is not so clear as in C-series. However, those of P4031

subjected to biaxial bending become worse, and obvious strength deterioration is observed in the hysteresis loop of P4031 compared with P4011 and P4000.

c) Failure modes

Two types of failure mode are observed in C-series specimens: In the first type, the plastic hinge formed at the top of the lower column only, and symmetrical doglegged configurations repeatedly appears in the positive and the negative loading, which is observed in C4000 only. In the second type, the ends of both upper and lower columns are plastified, and the doglegged configuration never recovers once it occurs one-direction, as observed in C4011, C4031 and C8031. The horizontal movement of the connection accumulates in one-direction with the repetition of the load. Therefore, three-dimensional loading on column-failing type specimen causes the unstable failure mode.

All specimens of P-series except P8031 exhibit large symmetrical deformation, showing the first type of failure mode mentioned above. Damage of concrete of these specimens somewhat scatters in the lower and the upper column and connection between beam A and column. It may be said that panel-failing specimen shows more stable failure mode than column-failing specimen. The effect of three-dimensional loading is not clear. P8031 collapses in the similar way as observed in C-series subjected to three-dimensional loading, and it does not exhibit the symmetrical deformation like other specimens in P-series, because of the large P-Δ effect.

4. CONCLUDING REMARKS

New findings obtained from the experiment on elasto-plastic behavior of steel reinforced concrete space frames are as follows:

(1) Maximum strength of any specimen in C-series attained in the positve loading cycle does not reach the calculated ultimate strength, although the maximum strength in the negative loading cycle exceeds the calculated value in some cases. P-Δ effect due to the movement of the connection must be considered in the calculation.

(2) Maximum strength of the specimens subjected to uniaxial bending in P-series is well estimated by the ultimate strength corresponding to the shear failure of the beam-to-column connection panel, and the strength of the other specimens subjected to biaxial bending could not reach the ultimate strength . Therefore, it is confirmed that the strength of the connection panel is decreased by the effects of biaxial bending.

(3) Hysteresis loops of all specimens show the pinched-shape at first few cycles of loading, and then they gradually shift to the spindle shape.

(4) Among the specimens in C-series, the deformation capacity and energy dissipation capacity of C4000 is much larger than others, and C8031 shows rather brittle failure. Three-dimensional loading and biaxial bending decreases the deformation capacity and energy dissipation capacity.

(5) The deformation capacity and energy dissipation capacity of P-series specimens are better than C-series specimens. The panel-failing type may be more advantageous than the column-failing type. The effect of three-dimensional loading is not so clear as in C-series.

(6) Two types of failure mode are observed: In the first type, symmetrical doglegged configurations repeatedly appears in the positive and the negative loading, and the beam-to-column connection symmetrically moves back and forth on the horizontal line. In the second type, the doglegged configuration never recovers once it occurs one-direction, and the horizontal movement of the connection accumulates in one-direction.
(7) Specimens in P-series except P8031 exhibit large symmetrical deformation, showing the first type of failure mode, and specimen in C-series exccept for C4000 exhibit the second type of failure mode. Three-dimensional loading on column-failing type specimen causes the unstable failure mode. The effect of three-dimensional loading is not clear in panel-failing specimens.

Acknowledgments The authors wish to express their sincere gratitude to Messrs. Junichi Honda (Sumitomo Construction Co.) and Takuya Yamamoto (Mie University), who helped in the experiments of this investigation.

References

[1] Stevens, R. F., "Encased Stanchions", The Structural Engineer, Vol. 43, Jan., 1965, pp. 59-66.
[2] Bridge, R. Q. and Roderick, W. J., "Behavior of Built-up Composite Columns", Journal of the Structural Division, ASCE, Vol. 104, No. ST7, July, 1978, pp.1141-1155.
[3] Morino, S., Matsui, C. and Watanabe, H., "Strength of Biaxially Loaded SRC Columns", Proc. of the U.S.-Japan Seminar on Composite and Mixed Construction, ASCE, 1985, pp. 185-194.
[4] Morino, S., Uchida, Y. and Ozaki, M., " Experimental Study on the Behavior of SRC Beam-Columns Subjected to Biaxial Bending", Proc. of Engineering Foundation Conference on Composite Construction in Steel and Concrete, ASCE, 1988, pp. 753-772
[5] Wakabayashi, M. and Minami, K., " Recent Experimental Studies on the Hysteretic characteristics of Beam-to-Column Connections in Composite Structures", Proc. of U.S.-Japan Seminar on Composite Structures and Mixed Structural Systems, St. Louis, Aug., 1980, pp. 217-226.
[6] Wakabayashi, M. and Minami, K., "Review of the Studies on the Shear Resistance of Composite Steel and Reinforced Concrete Beam-to-Column connections", Preprint of U.S.-New Zealand-Japan Seminar, Monterey, July, 1984.
[7] Kozai Club, "Design Manual of H-Shaped Steel for SRC Structures", Kozai Club, Tokyo, 1984.
[8] Matsui, C., Morino, S. and Ueda, Y., "Maximum Strength of Steel Reinforced Concrete Section Subjected to Axial Thrust and Biaxial Bending", Technology Reports of Kyushu University, Vol.57, No.2, March, 1984, pp. 95-101.
[9] Architectural Insutitute of Japan, "Standard for Structural Calculation of Steel Reinforced Concrete Structures", AIJ, 1987.

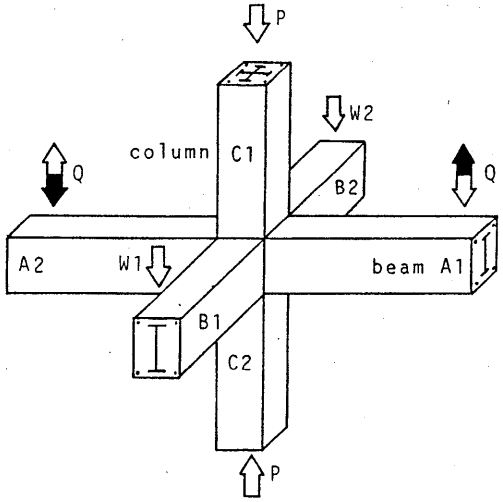

Fig. 1 Schematical view of test

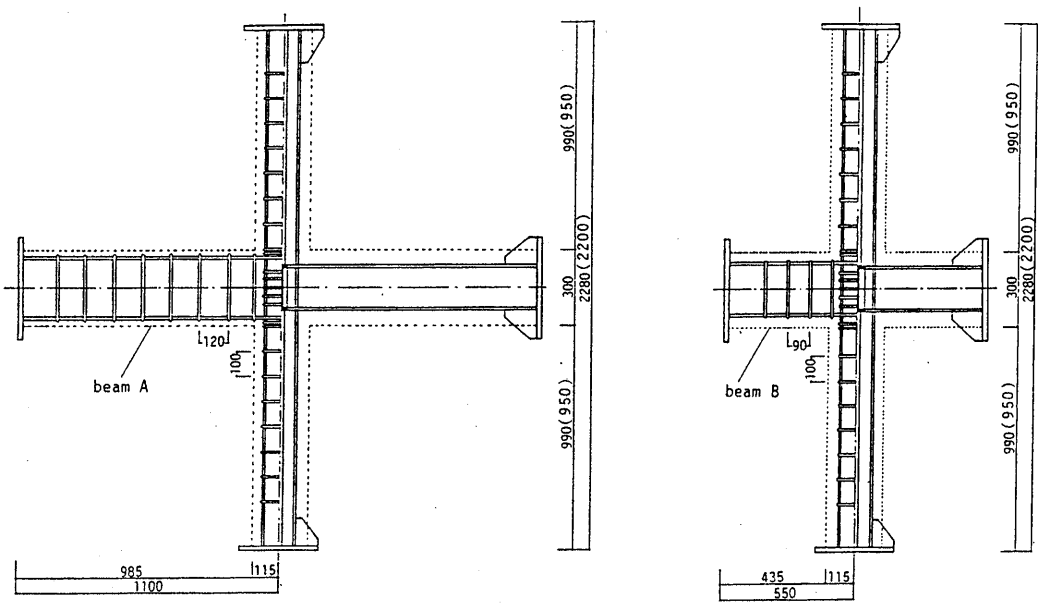

Fig. 2 Details of specimen
(Numbers in parenthesis are for P-series specimens)

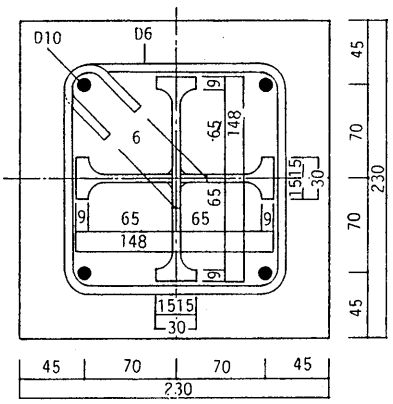

(a) column

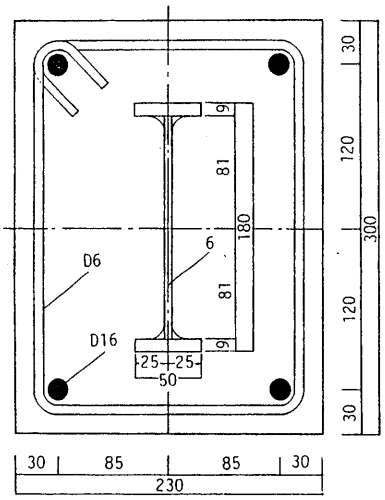

(b) beam A

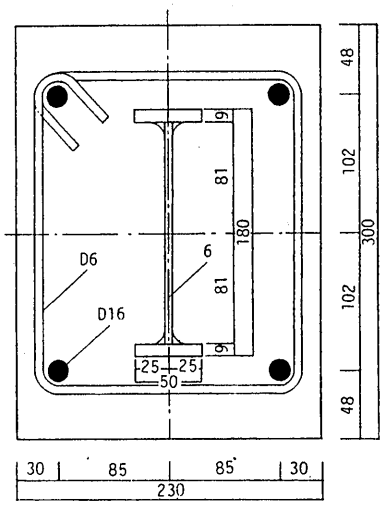

(c) beam B

Fig. 3 Cross section of specimen

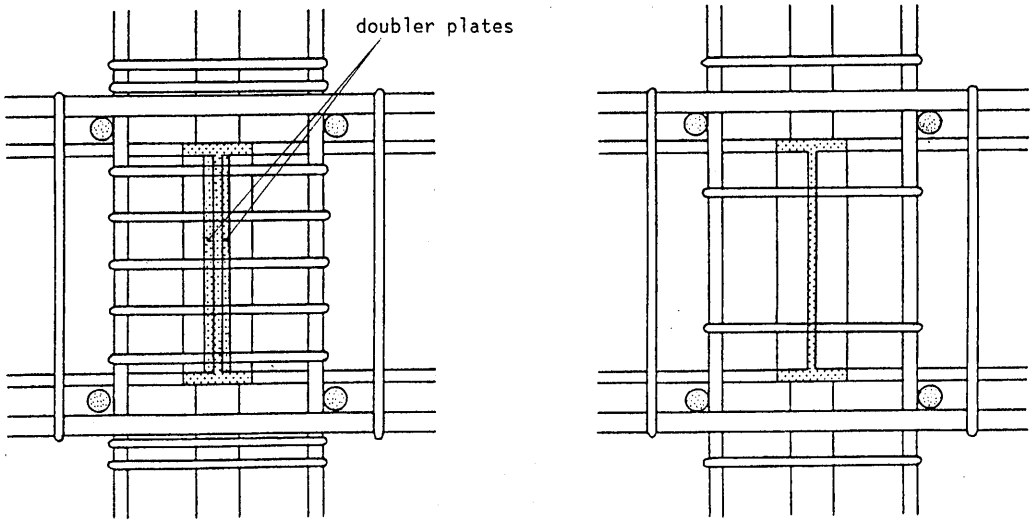

(a) C-series (b) P-series

Fig. 4 Details of connection panel

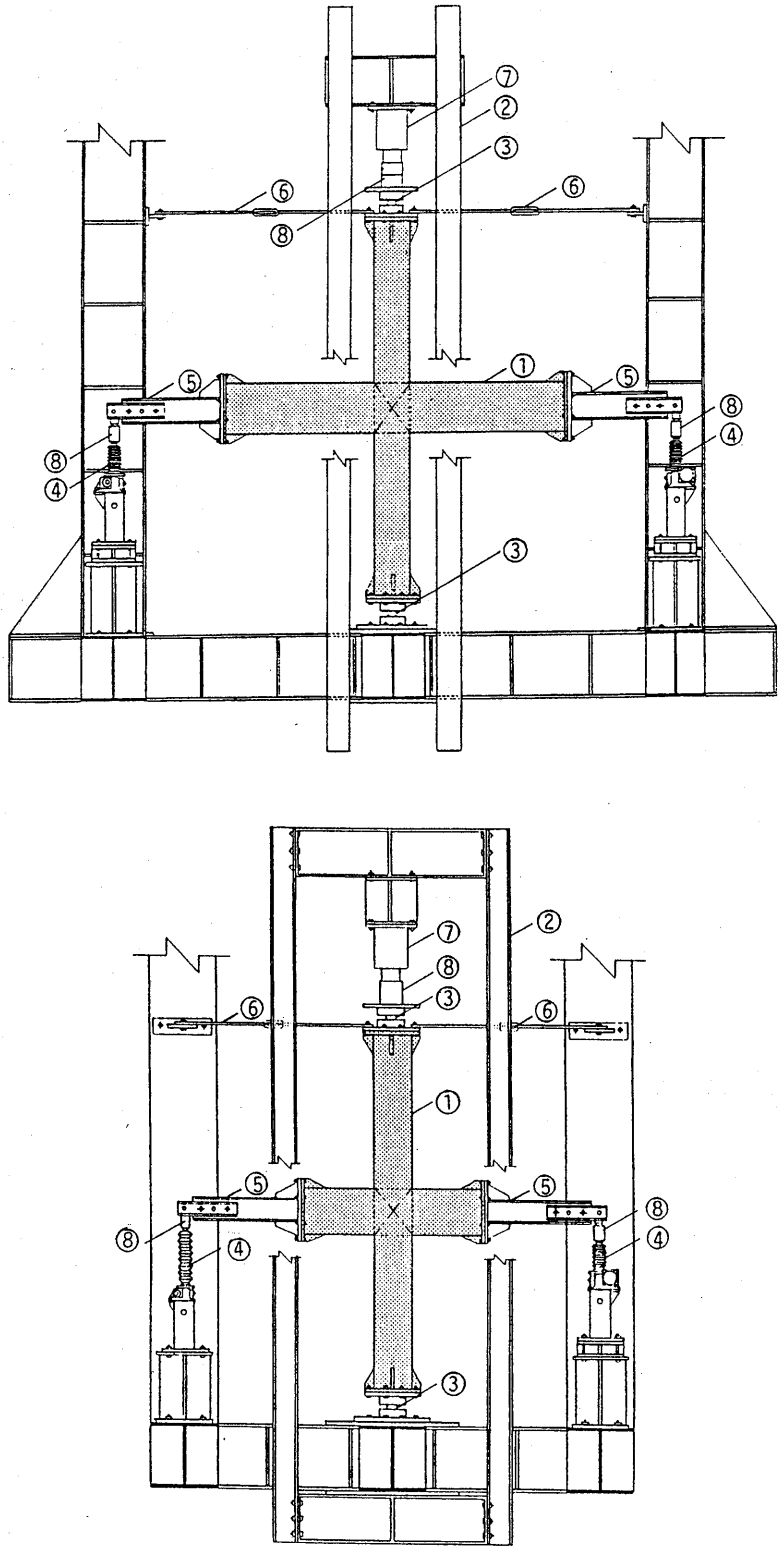

Fig. 5 Test set-up

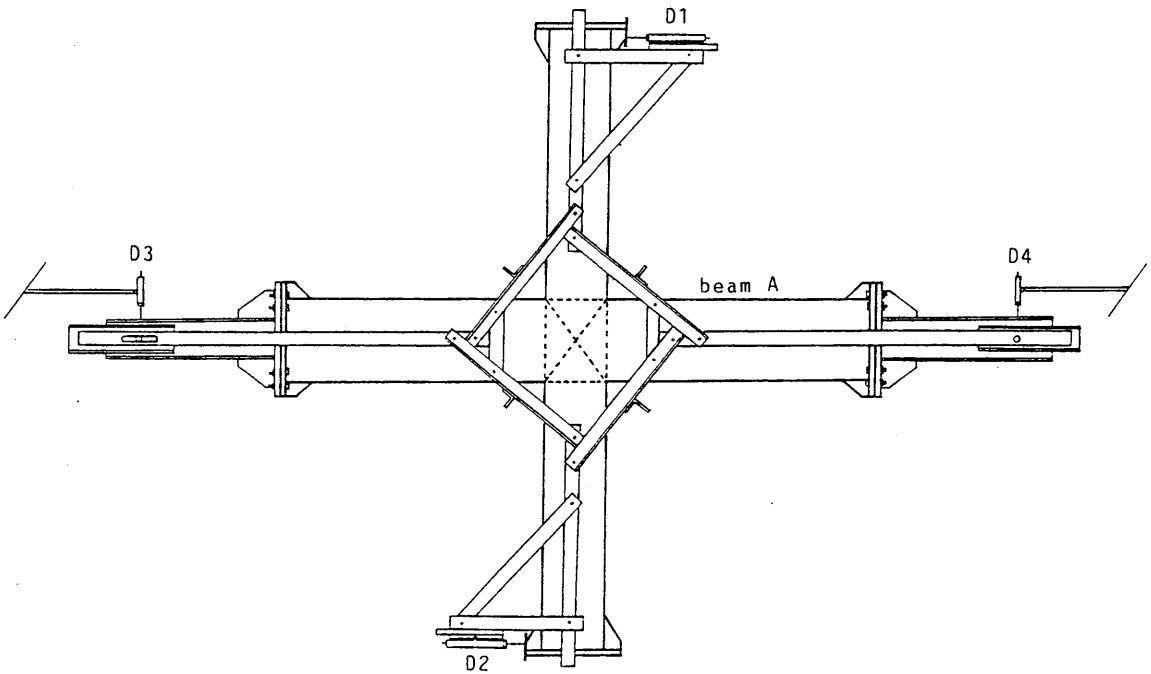

Fig. 6 Displacement measuring system

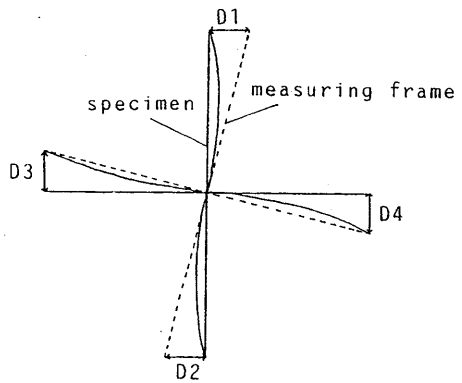

Fig. 7 Deformed specimen and measuring frame

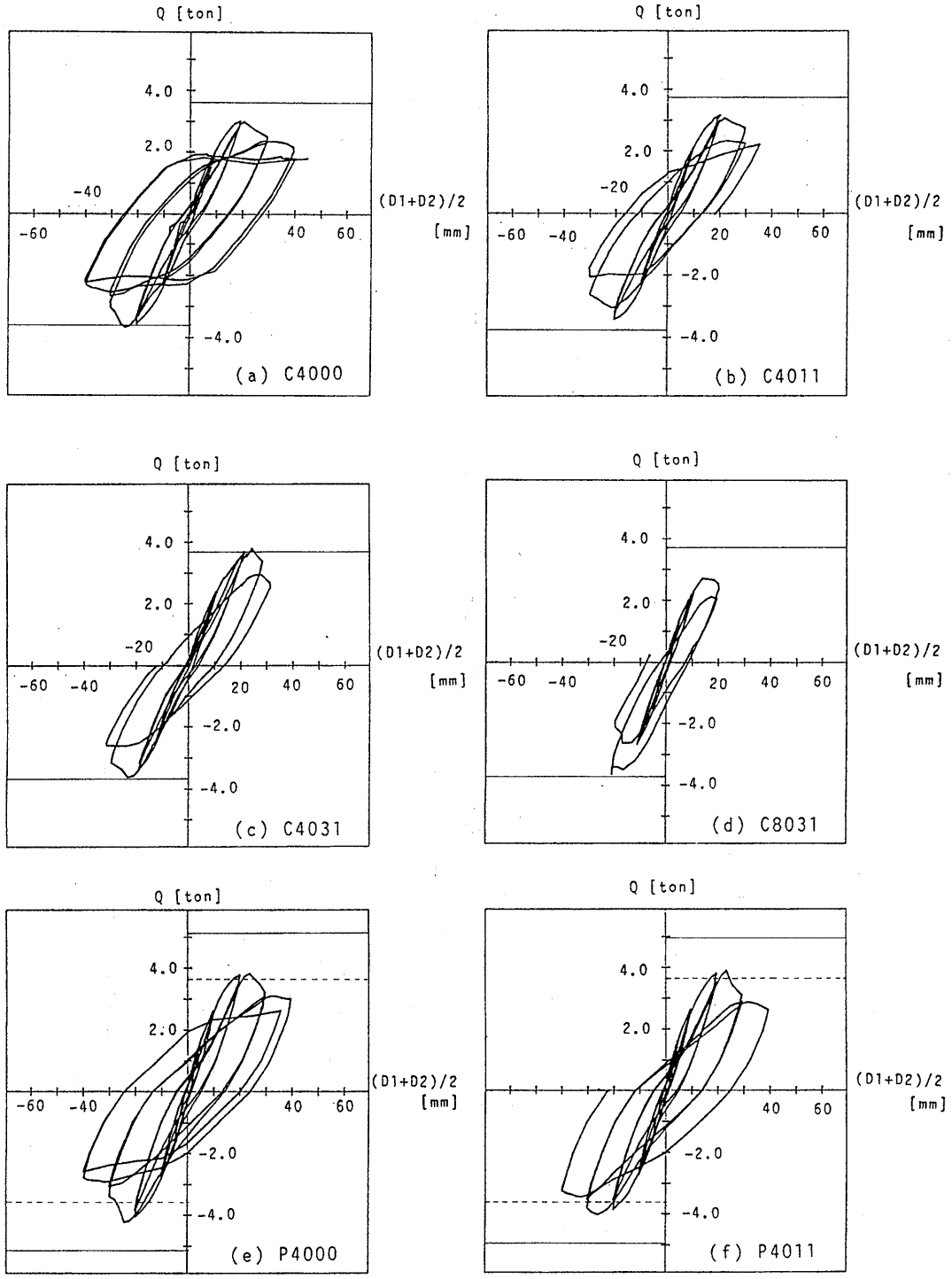

Fig. 8 Relasions between load and average displacement of column

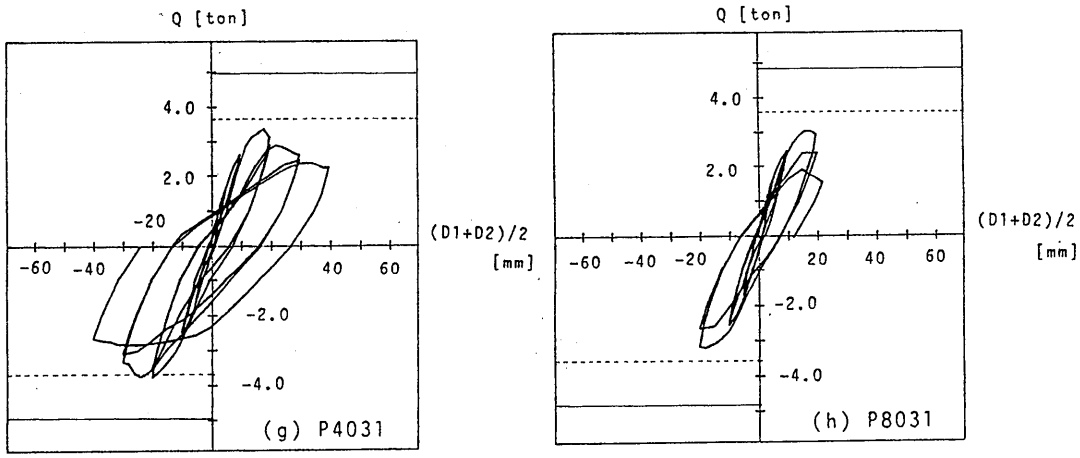

Fig. 8 Relations between load and average displacement of column (continued)

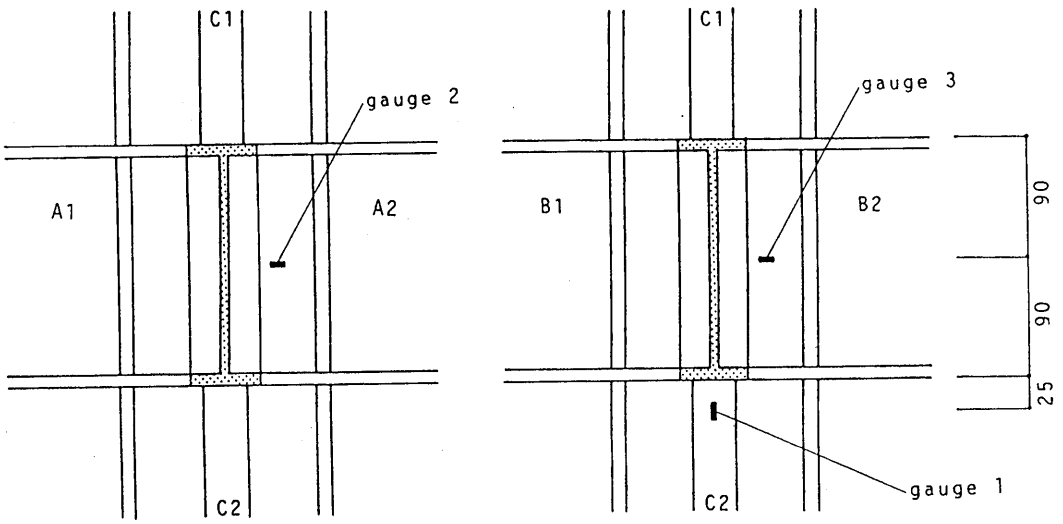

Fig. 9 Locations of wire strain gauges

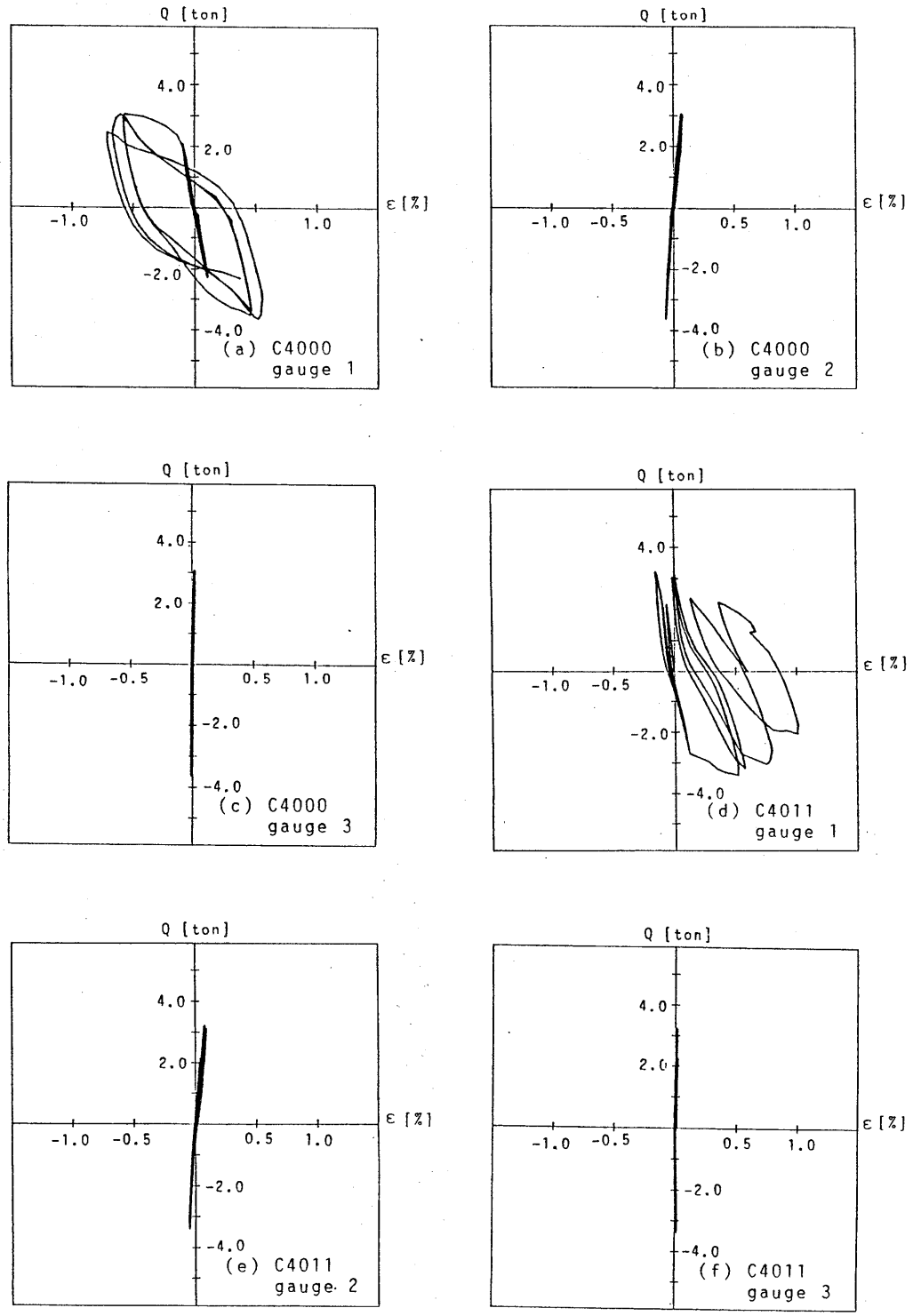

Fig. 10 Load-strain relations

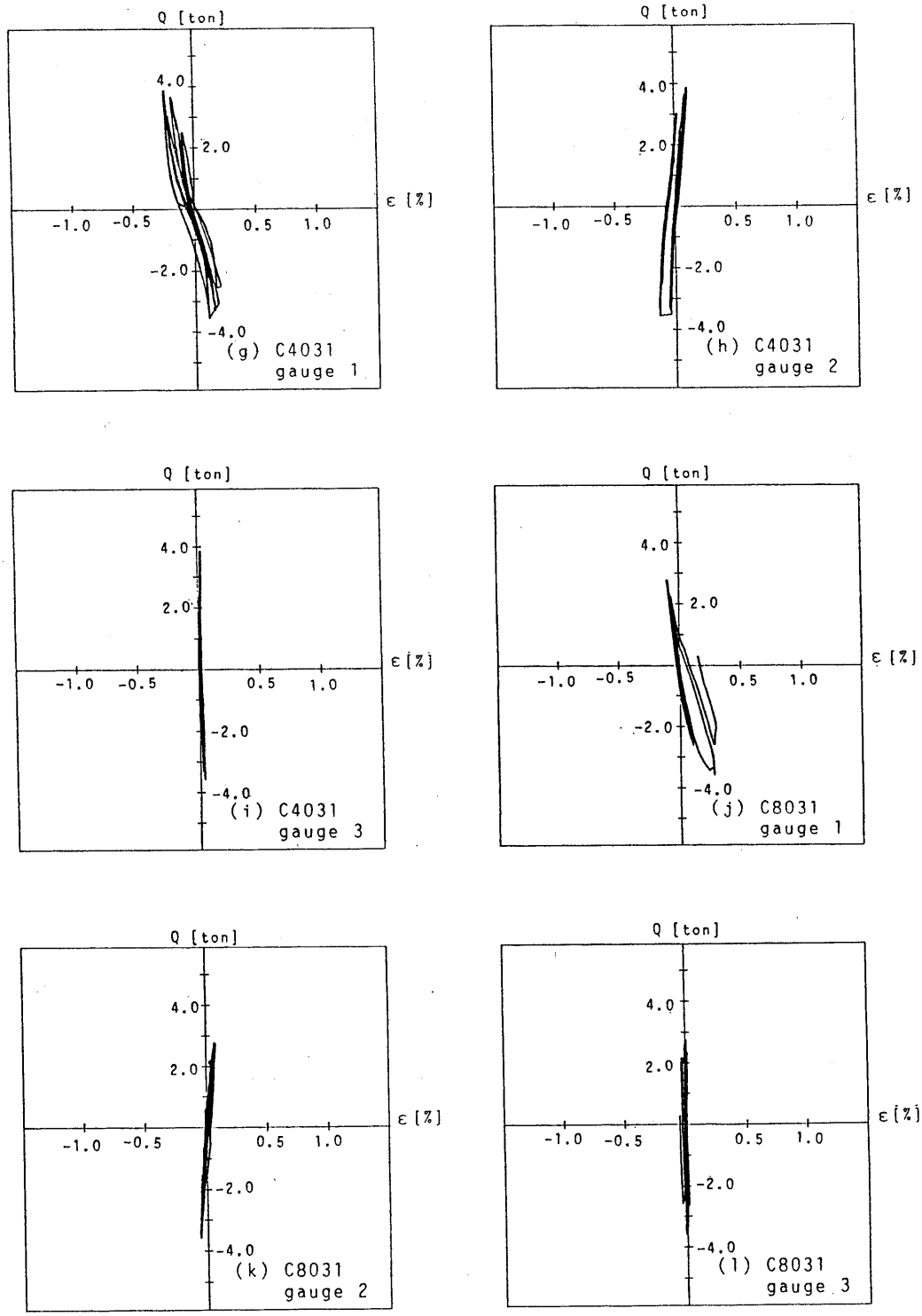

Fig. 10 Load-strain relations (continued)

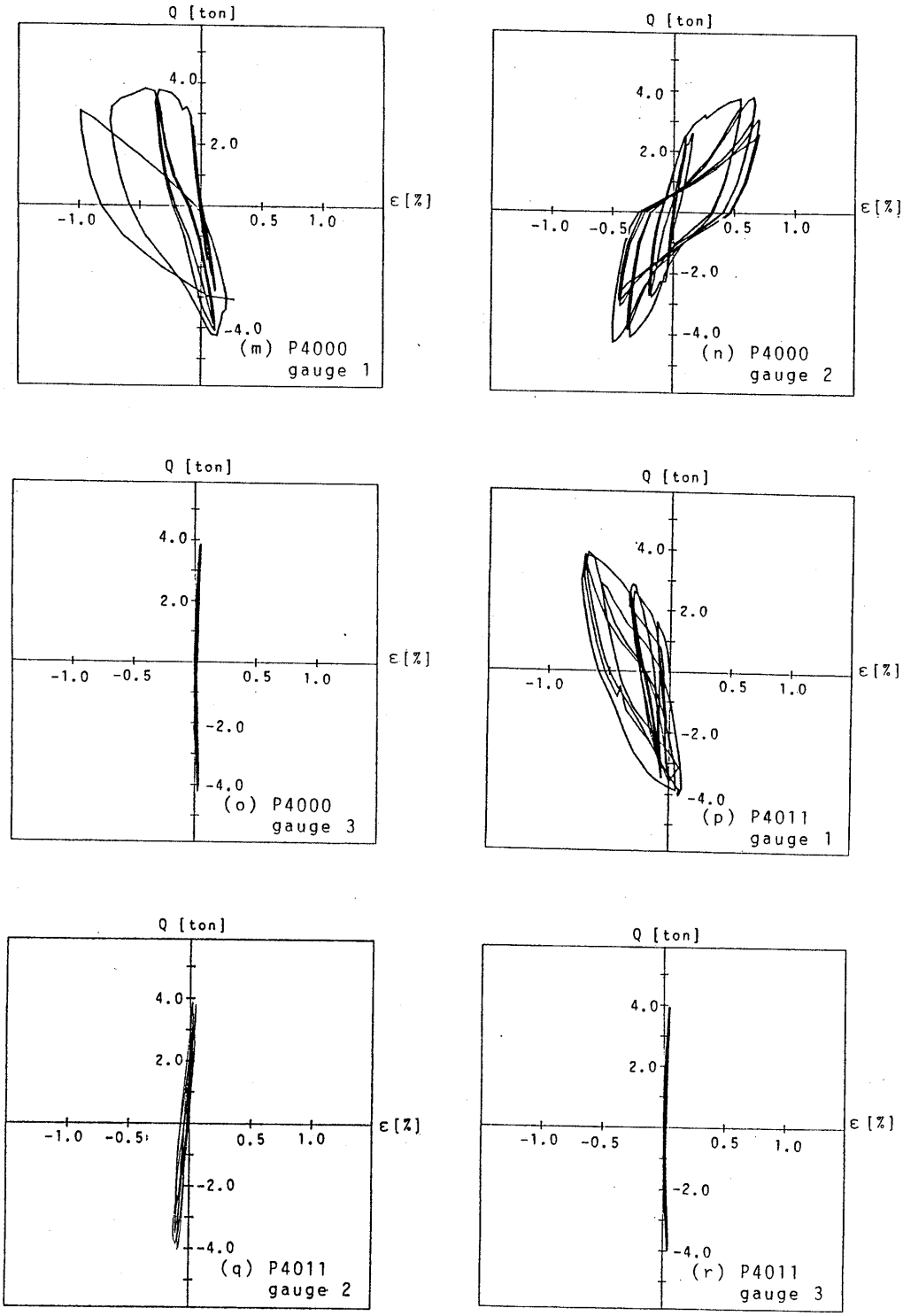

Fig. 10 Load-strain relations
(continued)

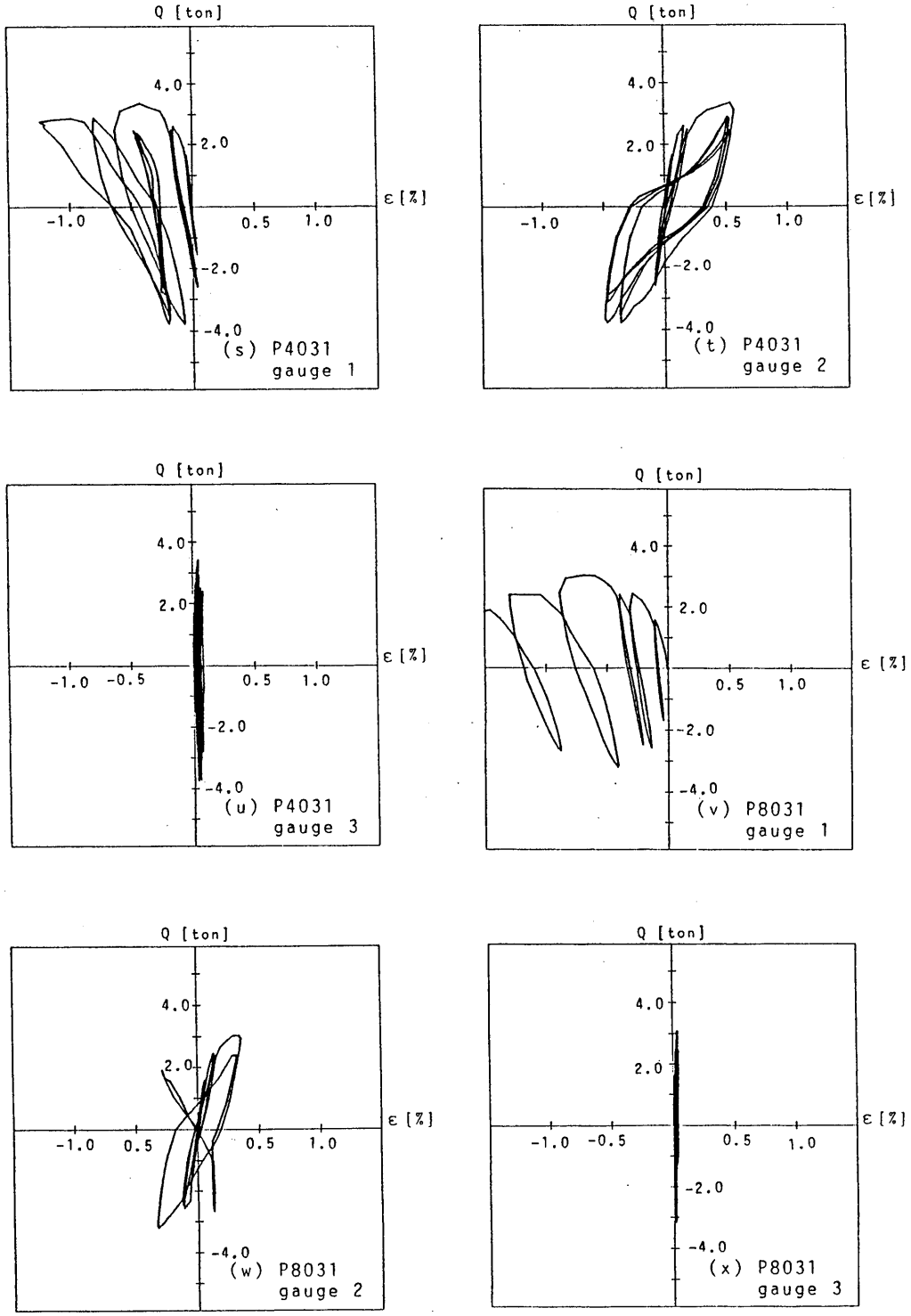

Fig. 10 Load-strain relations (continued)

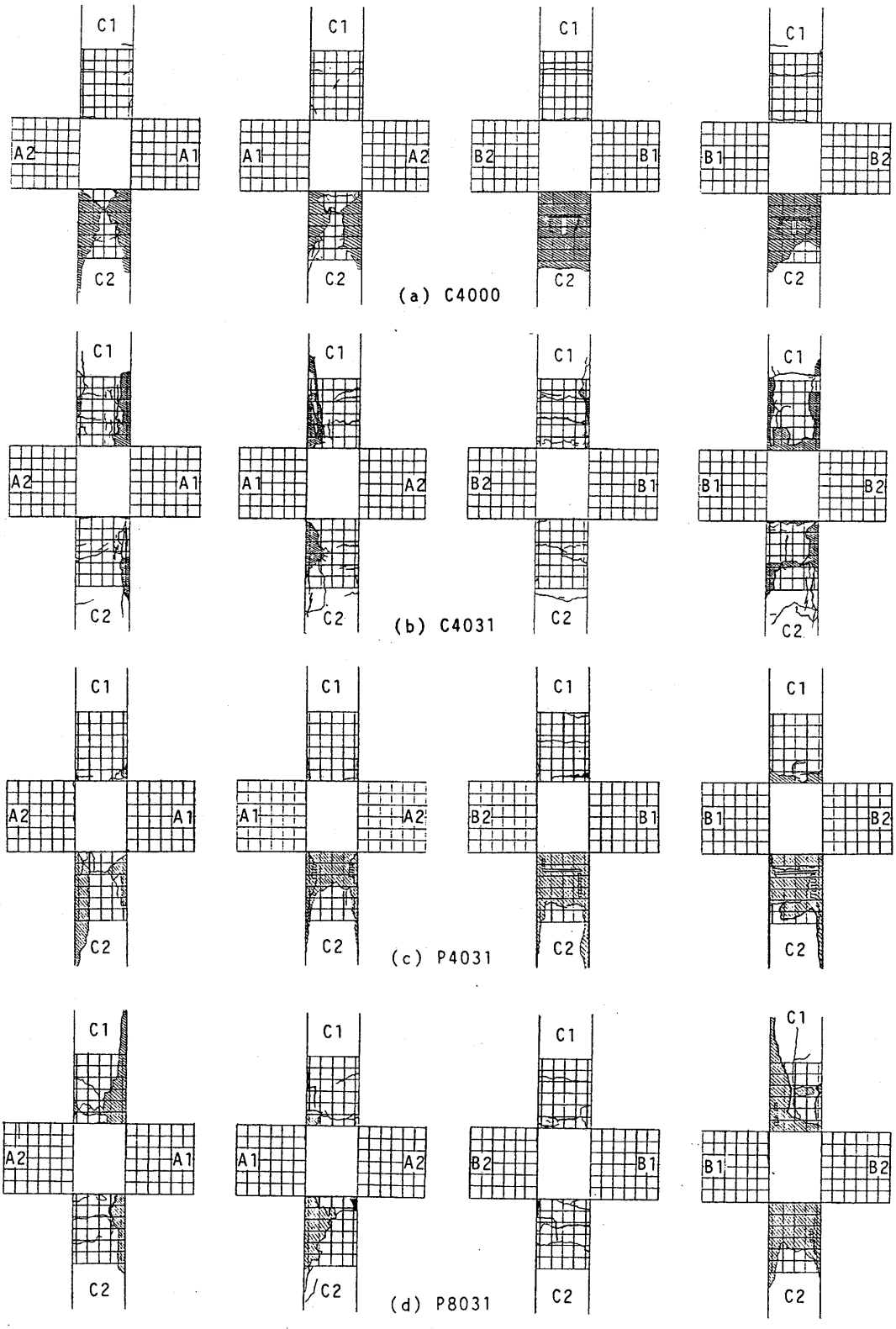

Fig. 11 Crack patterns

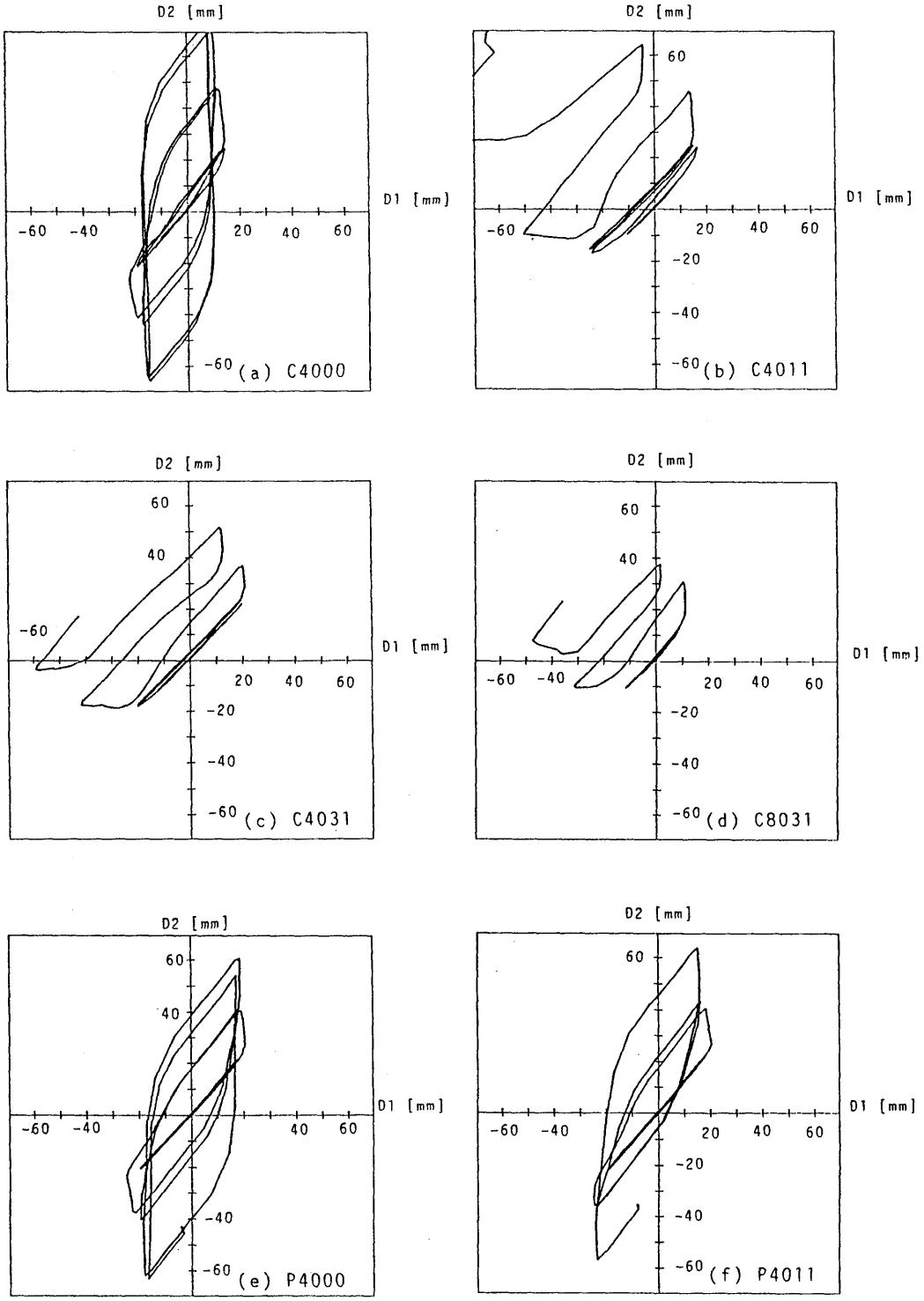

Fig. 12 Relations between displacements at top and base of column

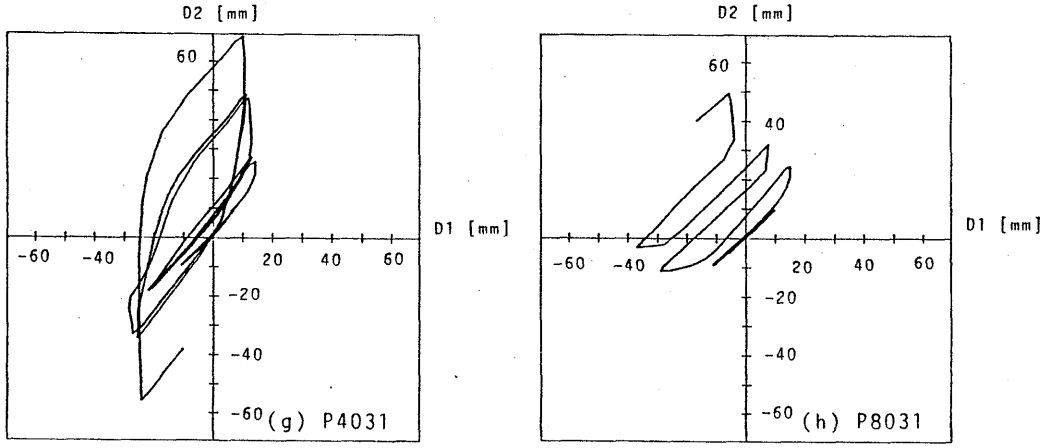

Fig. 12 Relations between displacements at top and base of column (continued)

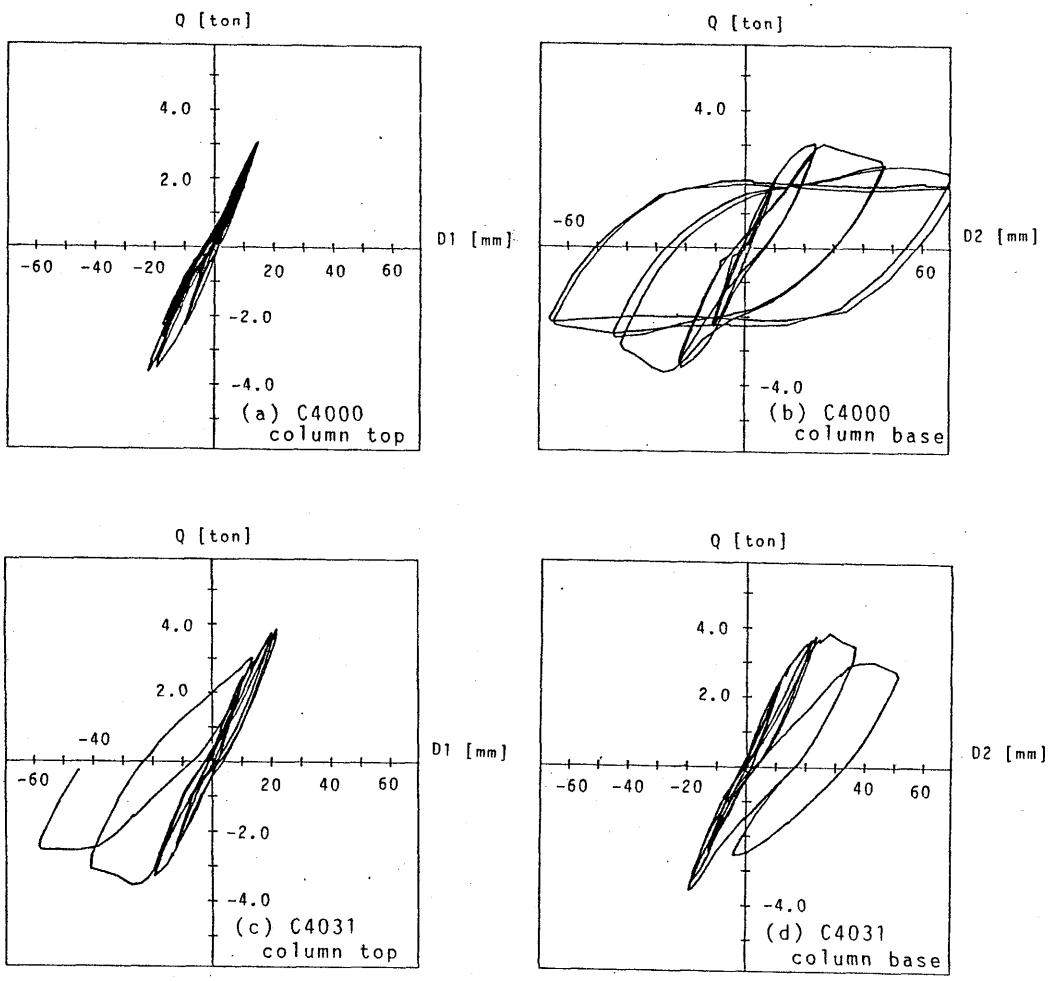

Fig. 13 Relations between load and column displacement

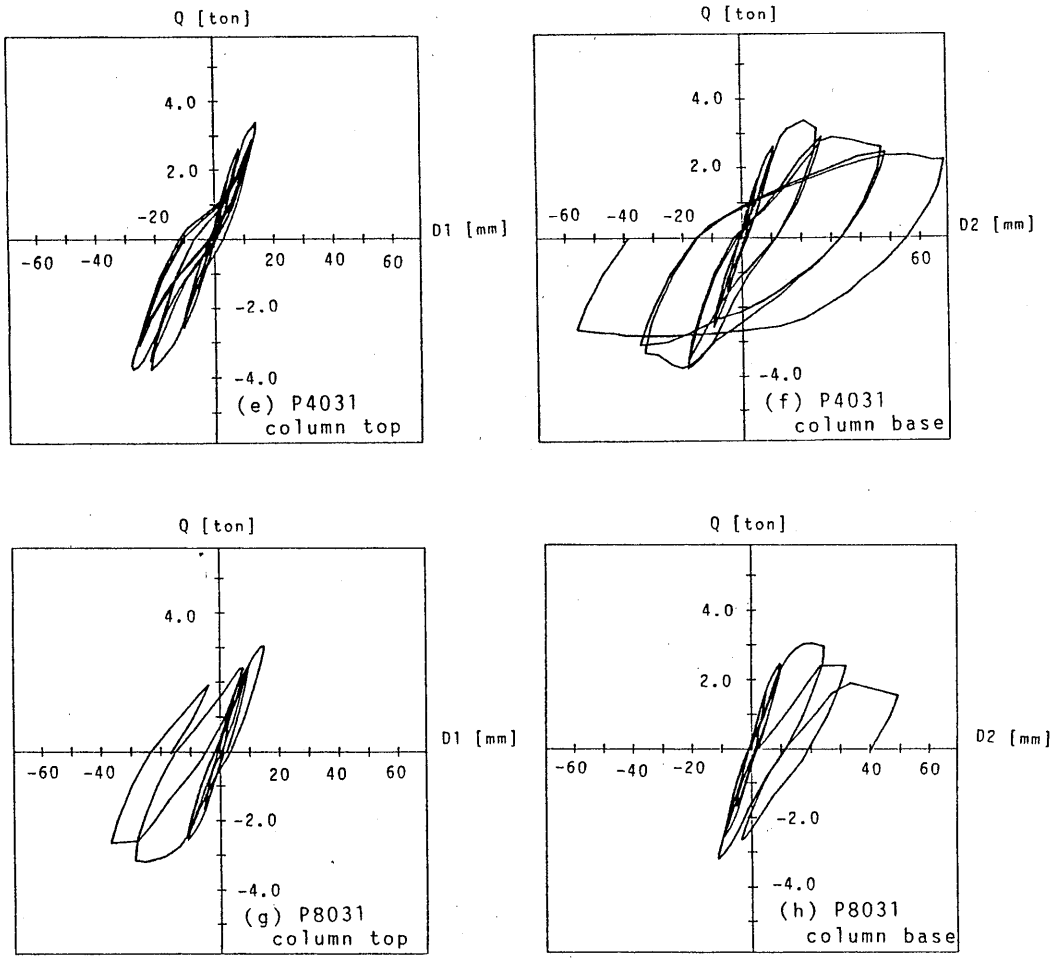

Fig. 13 Relations between load and column displacement (continued)

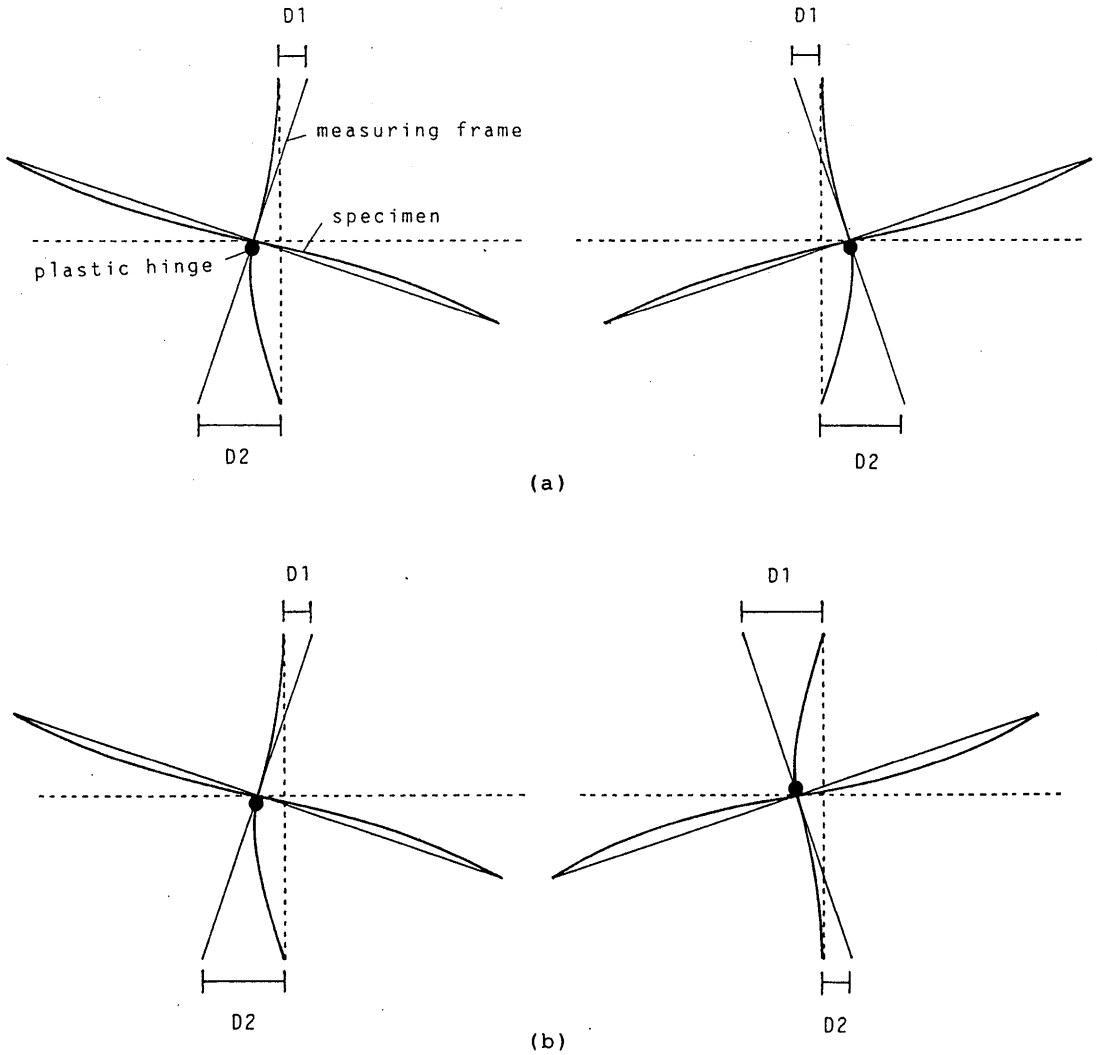

Fig. 14 Deformed configurations of columns

Table 1 Name of specimen

specimen	P *1	W1, W2 *2	failure mode
C4000	40 (20)	0, 0	column
C4011	40 (20)	1, 1	column
C4031	40 (20)	3, 1	column
C8031	80 (40)	3, 1	column
P4000	40 (15)	0, 0	panel
P4011	40 (15)	1, 1	panel
P4031	40 (15)	3, 1	panel
P8031	80 (30)	3, 1	panel

*1 constant axial thrust (ton), and ratio to ultimate axial thrust in parenthesis (%)
*2 beam B load simulating the long-term loading (ton)

Table 2 Material properties

(a) steel

		σ_y *1	σ_u *2	ε *3
C-series	column frange	3562.0	4865.7	20.59
	column web	4135.0	5073.7	18.84
	panel plate(6mm)	3356.8	4274.4	27.75
	steel bar D10	3274.6	4827.5	21.03
P-series	column frange	3622.0	4984.5	22.87
	column web	4215.0	5195.5	16.70
	panel plate(6mm)	2845.3	4060.6	24.65
	steel bar D10	3606.4	5305.0	20.11
	D 6	3885.4	5351.0	-

*1 yeild stress (kg/cm^2)
*2 ultimate tension strength (kg/cm^2)
*3 elongation (%)

(b) concrete

specimen	cylinder strength (kg/cm^2)	specimen	cylinder strength (kg/cm^2)
C4000	184.8	P4000	363.2
C4011	213.9	P4011	345.6
C4031	196.7	P4031	357.6
C8031	201.5	P8031	333.6

Table 3 Measured dimensions of column and panel

specimen	D_c	b_c	d_s	b_s	t_f	t_w	d_p	b_p	t_p
C4000	230.8	231.1	149.7	30.5	9.07	5.54	162.06	131.46	18.23
C4011	231.5	231.4	149.2	31.3	8.81	6.26	161.30	131.04	18.68
C4031	233.2	232.1	149.3	29.8	8.86	5.66	161.73	131.62	18.50
C8031	230.5	231.1	149.9	30.5	8.92	5.62	161.80	131.17	18.40
P4000	232.0	229.0	147.9	30.5	8.41	5.81	162.91	131.36	5.75
P4011	231.3	231.8	147.8	30.9	8.53	5.79	162.03	130.88	5.90
P4031	230.5	231.3	147.4	30.4	8.45	5.53	162.24	131.35	5.70
P8031	231.0	228.8	147.7	29.9	8.48	5.57	162.41	131.24	5.63

D_c : depth of concrete section
b_c : width of concrete section
d_s : depth of steel section
b_s : width of steel flange
t_f : thickness of flange
t_w : thickness of web
d_p : depth of panel plate
b_p : width of pannel plate
t_p : thickness of panel plate

Dimensions of steel portion shown above are the average for cross-shaped column section. Unit: mm